Journal of Hazardous Materials 189 (2011) 821–826

Contents lists available at ScienceDirect

Journal of Hazardous Materials

journal homepage: www.elsevier.com/locate/jhazmat

An investigation into the electrochemical recovery of rare earth ions in a CsCl-based molten salt

Shuqiang Jiao*, Hongmin Zhu*

School of Metallurgical and Ecological Engineering, University of Science and Technology Beijing, Beijing, 100083, PR China

ARTICLE INFO

Article history:
Received 13 January 2011
Received in revised form 4 March 2011
Accepted 9 March 2011
Available online 16 March 2011

Keywords:
Rare earth
Cyclic voltammetry
Square wave voltammetry
Cathodic process
E-pO^{2-} diagram

ABSTRACT

A CsCl-based melt, was used as a supporting electrolyte for a fuel cycle in pyrochemical separation, as it has a high solubility for lanthanide oxide. Cyclic voltammetry and square wave voltammetry were carried out to investigate the cathodic reduction of those rare earth ions. The results prove that the cathodic process of La(III) ions dissolved in a CsCl-based melt, with a one-step reduction $La^{3+} + 3e^- = La$, and is similar to those of other reports which have utilised LiCl–KCl or $CaCl_2$–KCl molten salt systems. However, for the Ce(III) ions that dissolved in a CsCl-based melt, there is a significant difference when compared with published literature as there are two reduction steps instead of the reported single step $Ce^{3+} + e^- = Ce^{2+}$ and $Ce^{2+} + 2e^- = Ce$. In order to explain the novel result, a detailed investigation was focused on the cathodic process of Ce(III) in a CsCl-based melt. The identification of the M–O (M = La, Ce) compounds that are stable in the electrolyte, as well as the determination of their solubility products, were carried out by potentiometric titration using an oxide ion sensor. Furthermore, the E-pO^{2-} (potential-oxide ion) diagram for the M–O stable compound was constructed by combining both theoretical and experimental data.

1. Introduction

Partitioning and transmutation (P&T) concepts have been extensively investigated as they have the potential to reduce the long-term radiotoxicity of nuclear waste [1–7]. Efficient recovery and multi-recycling of actinides and lanthanides are essential for P&T concepts. During the past decade, the pyrochemical separation process in molten media has been proposed as a promising future option for the nuclear fuel cycle. The alkali molten chlorides are particularly attractive for use as a solvent for those processes [8–15]. Hence, it is of importance that there is basic chemistry data for actinides and lanthanides in molten halogenide salts. Lanthanum and cerium are the most common lanthanide elements, and these have been investigated concerning their chemical and electrochemical behaviors in molten salts. A LiCl–KCl eutectic [9,10] and an equimolar mixture of $CaCl_2$–KCl [9] have often been hired as the solvent in most other research work. For the LiCl–KCl eutectic system and the equimolar mixture of NaCl–KCl, the electro-reduction of MCl_3 (M = La, Ce) at solid cathodes (W or Mo) occurs only in a single electrochemical step, which takes place near the potential of the alkaline electrodeposition [9,10].

A CsCl-based molten system has been considered the best solvent for use in pyrochemical separation, as it has a high solubility of the lanthanide oxide. In this work, we present a study on the chemical and electrochemical properties of rare earth chlorides (MCl_3, M = La, Ce) in the molten chloride mixture NaCl–2CsCl. Cyclic voltammetry (CV) and square wave voltammetry (SWV) were selected to investigate the cathodic processes of the lanthanum and cerium ions. Furthermore, square wave voltammetric results were used to construct calibration curves, as this technique is signified by its excellent sensitivity and high resolution [16,17]. It is clear from the experiment that square wave data is more accurate than cyclic voltammograms for such quantitative studies.

The E-pO^{2-} (potential-oxide ion) diagram for the M–O compound was constructed by combining both theoretical and experimental data. The best chlorinating condition could be extracted from comparison of the E-pO^{2-} diagram, corresponding to the M–O compounds and that of some chlorinating mixtures. The identification of the M–O (M = La, Ce) compounds that are stable in the NaCl–2CsCl melt, as well as the determination of their solubility products, were carried out by potentiometric titration using an oxide ion sensor.

2. Experimental

2.1. The cell, the electrode

All chemicals were of reagent grade quality. NaCl and CsCl were mixed at a molar ratio of 1:2 in a glove box, and were then charged into an alumina crucible. The electrolyte was melted in

* Corresponding authors.
E-mail addresses: sjiao@ustb.edu.cn (S. Jiao), hzhu@metall.ustb.edu.cn (H. Zhu).

0304-3894/$ – see front matter © 2011 Elsevier B.V. All rights reserved.
doi:10.1016/j.jhazmat.2011.03.027

the alumina crucible after being placed in a furnace controlled by a CHIND DI3000 programmable device. It should be noted that the experiments were performed in an inert U-grade argon atmosphere previously dehydrated by heating in a vacuum. The working temperature was measured by a thermocouple (protected by an alumina tube) that was inserted into the melt. All measurements were carried out under the atmosphere of dried nitrogen (above U-grade argon), and the temperature was fixed at 873 K.

The analytical electrochemical techniques used (cyclic voltammetry and square wave voltammetry) require a three-electrode set-up.

The working electrode was a tungsten wire with a diameter of 0.1 mm. The electrode was encapsulated in quartz, with the lower circular cross section exposed to the melt. The apparent area was 7.8×10^{-5} cm^2.

The reference electrode was an Ag/AgCl electrode, which consisting of a silver wire with a diameter of 1 mm contained in a Mulite tube, and dipped into a silver chloride solution (4 wt%) in the NaCl–CsCl molten mixture.

The auxiliary electrode was a graphite rod with a 6 mm diameter.

2.2. The electrochemical analysis methods

Cyclic voltammetry was initially applied to investigate the cathodic process of rare earth ions in a NaCl–2CsCl molten salt. Subsequently, square wave voltammetry, which has been described in detail by Osteryoung etc. [20–23], was selected for quantitative study. For square wave voltammetry for the ideal case of a reversible system, the potential–current curve has a Gaussian shape with a peak at a potential close to the half-wave potential for the ionised species. The mathematical expression has the following characteristics:

(i) The width of the peak ($W_{1/2}$) at half its height depends on the number of electrons (n) exchanged at the operating temperature.

$$W_{1/2} = 3.52\frac{RT}{nF} \quad (1)$$

where R is the ideal gas constant; T: absolute temperature; F: Faraday constant and 3.52 is dimensionless.

(ii) The peak current (i_p) varies linearly with the concentration of the electroactive species and with the square root of the frequency (f) according to the equation.

$$i_p = nFAC_0\frac{1-\Gamma}{1+\Gamma}\sqrt{\frac{Df}{\pi}} \quad \Gamma = \exp\left(\frac{nF\Delta E}{2RT}\right) \quad (2)$$

where ΔE is the amplitude of the square wave potential; A: surface area of electrode; D: diffusion coefficient; C_0: bulk concentration of the electroactive species.

2.3. Instrumentation

The electrochemical experiments were performed using a PAR Model 263 potentiostat/galvanostat connected with a computer.

2.4. Potentiometric titration

A magnesia stabilised zirconia tube with an inner reference of Cr/Cr_2O_3 was used for the oxide sensor, while a Ag/AgCl electrode was used as the reference electrode, solid NaOH was used as the source of O^{2-} to titrate the M(III) (M = La, Ce). The *emf* was measured with a high impedance multimeter.

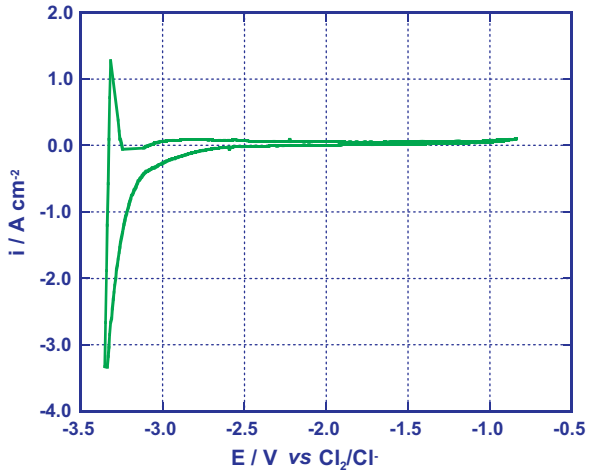

Fig. 1. A potential window of a cyclic voltammogram in a NaCl–2CsCl melt with a scan rate of 0.6 V s^{-1}.

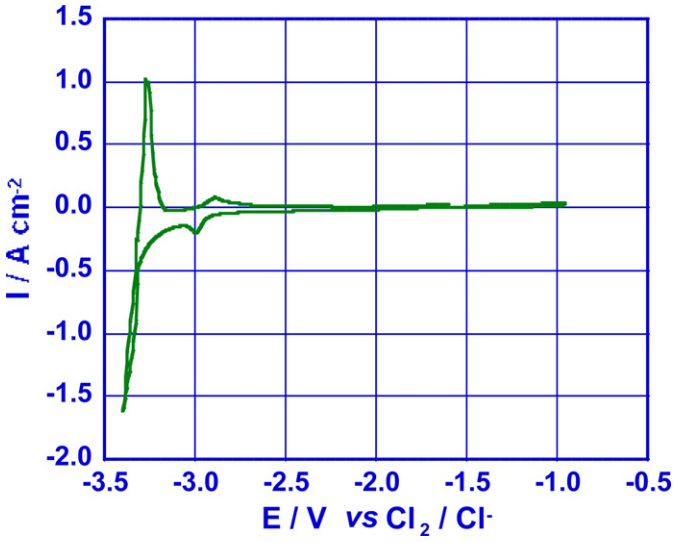

Fig. 2. A typical cyclic voltammogram performed in a NaCl–2CsCl melt with a 103 mM lanthanum trichloride. A scan rate of 0.6 V s^{-1} was used.

3. Results and discussion

A potential scan was performed in the purified NaCl–2CsCl melt using a tungsten microdisk electrode, and the potential window was subsequently recorded (Fig. 1). It is clear that there are no peaks on the voltammogram during the negative potential scan until the electrodeposition of sodium.

A 103 mM lanthanum trichloride was added into the NaCl–2CsCl melt, and then the electrochemical investigation was carried out. Figs. 2 and 3 show the typical cyclic and square wave voltammograms obtained. In the negative potential scan, only one cathodic peak appears at 3.0 V (*vs* Cl_2/Cl^-) on the both voltammograms. The current–potential curve in Fig. 3 is bell-shaped and symmetrical about the half-wave potential, and the peak can be used for quantitative analysis. Once again, this demonstrates the significant advantage of square wave voltammetry with respect to cyclic voltammetry, and its ability to accurately quantify an electrochemical process. The exchange electron number was calculated as 3 through the peak parameters. The electro-reduction reaction of lanthanum trichloride in a NaCl–2CsCl melt should proceed through the following equation:

$$La^{3+} + 3e^- = La \quad (3)$$

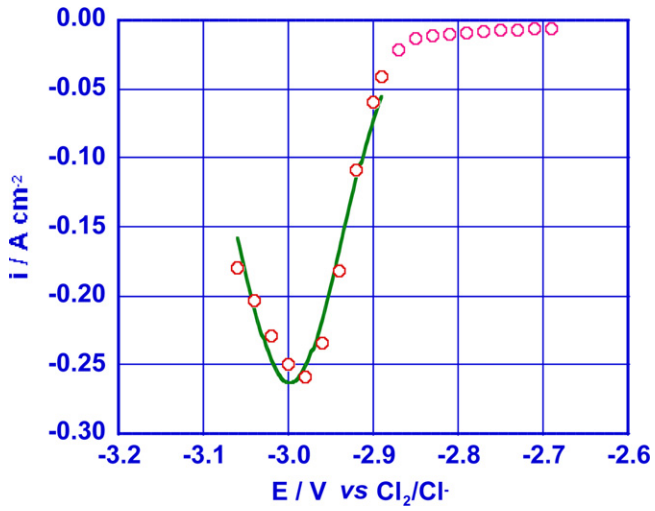

Fig. 3. A typical square wave voltammogram recorded in a NaCl–2CsCl melt with a 103 mM lanthanum trichloride. The square wave amplitude was 20 mV, while the frequency was 50 Hz.

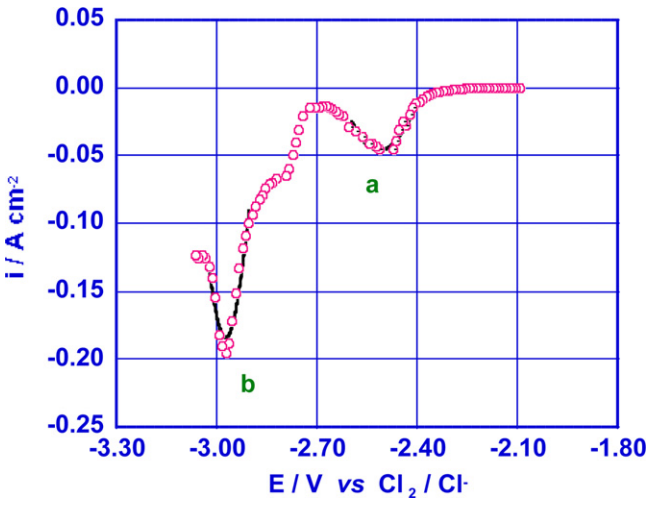

Fig. 5. A typical square wave voltammogram recorded in a NaCl–2CsCl melt with a 128 mM cerium trichloride. The square wave amplitude was 20 mV, while the frequency was 50 Hz.

which is similar to other researchers results obtained in LiCl–KCl [9,10], $CaCl_2$–KCl [9] etc. molten salts.

However, a significant difference occured for the study using cerium trichloride. The result in Fig. 4 shows that in a NaCl–2CsCl melt with 128 mM $CeCl_3$, that there are two cathodic peaks, (A) and (B) on cyclic voltammogram, which are associated to the two sharp anodic peaks, (A′) and (B′) Furthermore, a typical square wave voltammogram is shown in Fig. 5. It is clear that there are two peaks during potential negative sweep. By measuring the width at mid-height of each peak, it is possible, using Eq. (1), to determine the electron number that must have been exchanged (n):

Peak (A): $n = 1$

Peak (B): $n = 2$

The calculated result proposes that (A) and (A′) correspond to a soluble–soluble system Ce(III)/Ce(II), while (B) and (B′) are associated with the formation of metallic Ce and its reoxidation. It can thus be concluded that the electro-reduction of Ce(III) ions in a NaCl–2CsCl molten salt proceeds via the following two-step process:

$$Ce^{3+} + e^- = Ce^{2+} \quad (4)$$

$$Ce^{2+} + 2e^- = Ce \quad (5)$$

This two-step mechanism is different from other authors working with LiCl–KCl, $CaCl_2$–KCl [9,10]. According to these authors, the electrochemical reduction of Ce(III) ions is a single step process.

For this reason, further studies involving the electro-reduction of Ce(III) ions in NaCl–2CsCl were carried out. Firstly, the influence of Ce(III) ion concentration was investigated. It is evident from Fig. 6 that the peak current increased with an increase in Ce(III) ion concentration. This information indicates that mass transport during the electrochemical reduction of Ce(III) ions may be the controlling process. For a Ce(III)/Ce(II) redox system (wave A and A′), the study of the voltammetric curves recorded at different potential scan rates (Fig. 7) shows that the peak potential keeps constant when changing the scan rate (for values up to 0.6 V s^{-1}). The result indicates that in these conditions (and after the correction of the ohmic drop), the mass transport is significantly lower than that corresponding to elec-

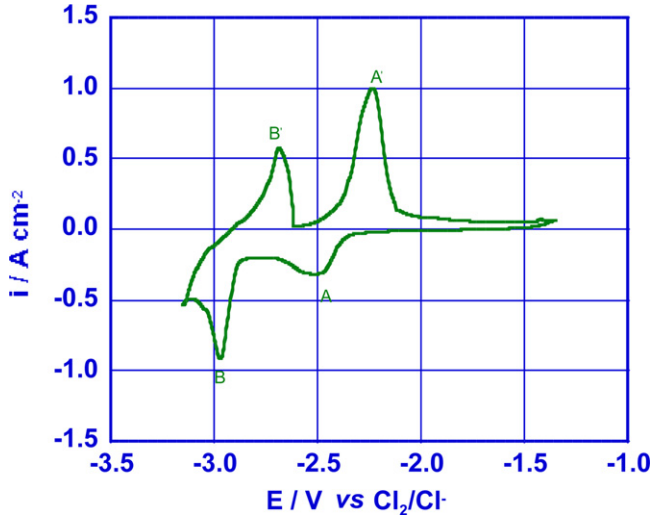

Fig. 4. A typical cyclic voltammogram performed in a NaCl–2CsCl melt with a 128 mM cerium trichloride. Scan rate was 0.6 V s^{-1}. Peak (A) and (A′) correspond to a soluble–soluble system Ce(III)/Ce(II), while (B) and (B′) are associated with the formation of metallic Ce and its reoxidation.

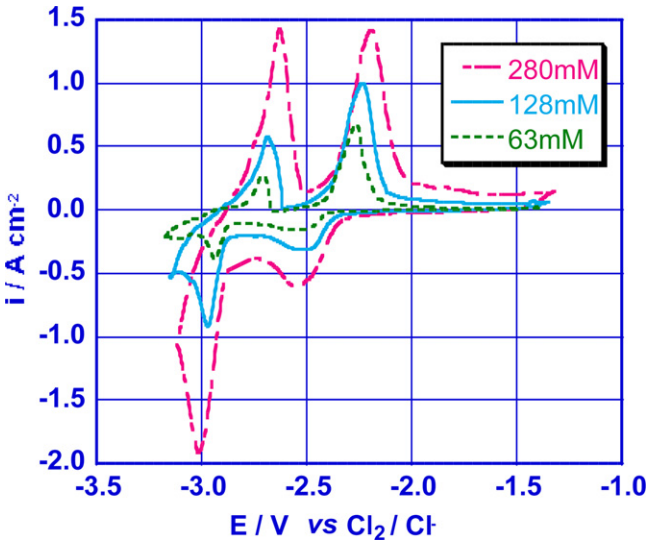

Fig. 6. The cyclic voltammograms performed in a NaCl–2CsCl melt including different concentrations of cerium trichloride. A scan rate of 0.6 V s^{-1} was used.

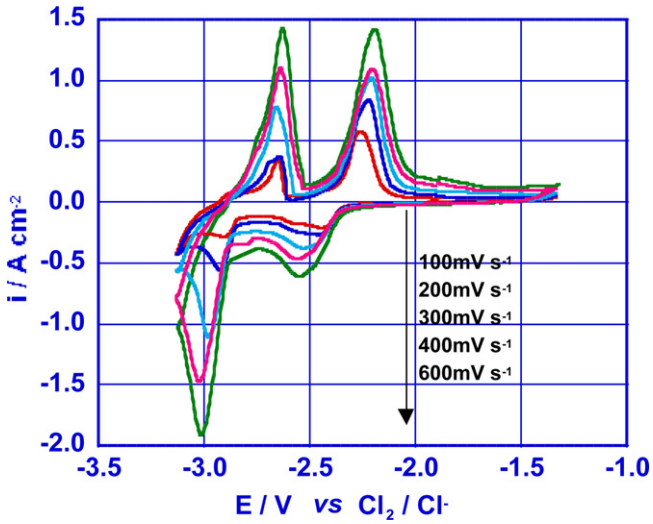

Fig. 7. The cyclic voltammograms with different scan rates in a NaCl–2CsCl melt with a 280 mM Ce(III) ion concentration.

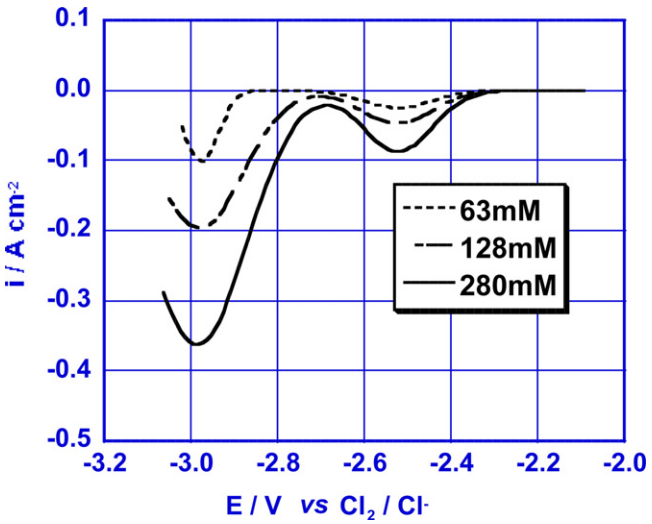

Fig. 9. The square wave voltammograms recorded for the different Ce(III) ion concentrations. The square wave amplitude was 20 mV, while the frequency was 50 Hz.

tron transfer. This phenomenon is indicative of electrochemical reversibility.

Fig. 8 highlights a directly proportional relationship between the current density of peak (A) and the square root of the potential scanning speed. From this linearity, it can be further concluded that this electrochemical reaction results in metal deposition controlled by semi-infinite linear diffusion; and from the proportionality factor, the diffusion coefficient for the Ce(III) species was calculated to be 6.23×10^{-5} cm^2 s^{-1}.

Following cyclic voltammetry, square wave voltammetry was also used to investigate the electro-reduction behavior of Ce(III) ions in a NaCl–2CsCl molten salt. The square wave voltammograms performed at different Ce(III) ion concentrations are given in Fig. 9. It is noticeable that the peak height is proportional to the concentration of the electroactive species.

According to Osteryoung and Barker [18–21], the height of the peak and the square root of frequency indicate the relationship as Eq. (2). By changing the frequency of a square wave signal, one can obtain a series of square wave voltammograms (Fig. 10). The reversibility can be checked by plotting the maximum current of the peak (A) versus the square root of the frequency of the square wave signal. The straight line obtained (see Fig. 11) confirms that

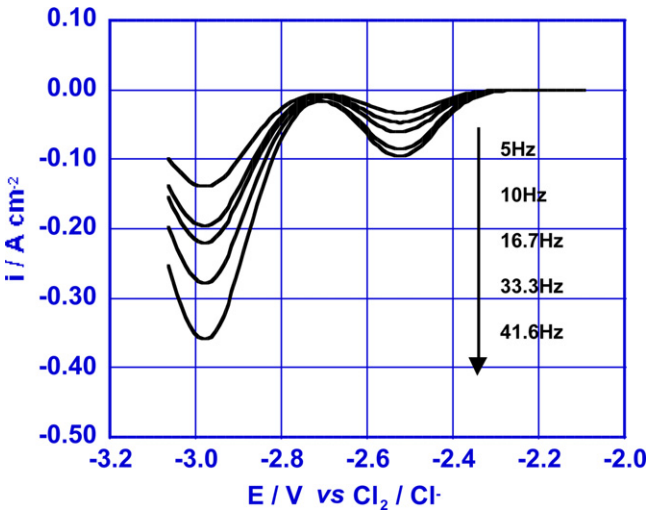

Fig. 10. Variation of the square wave voltammograms with the frequency. The square wave amplitude 20 mV, and the Ce(III) ion concentration 128 mM.

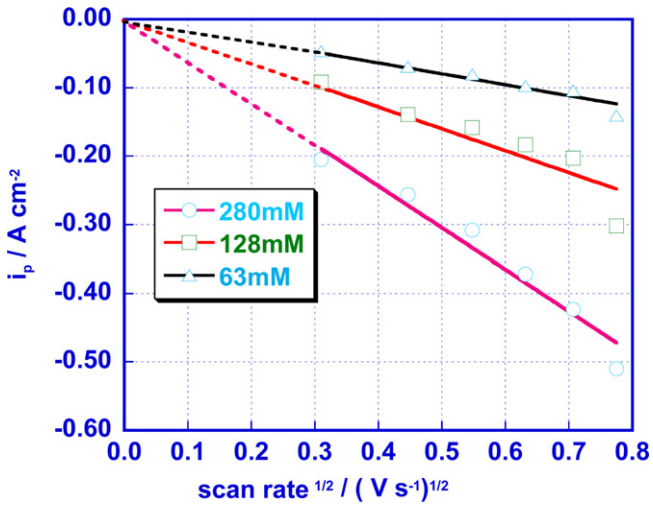

Fig. 8. The linear relationship between cathodic peak current (A) and square root of the scan rate.

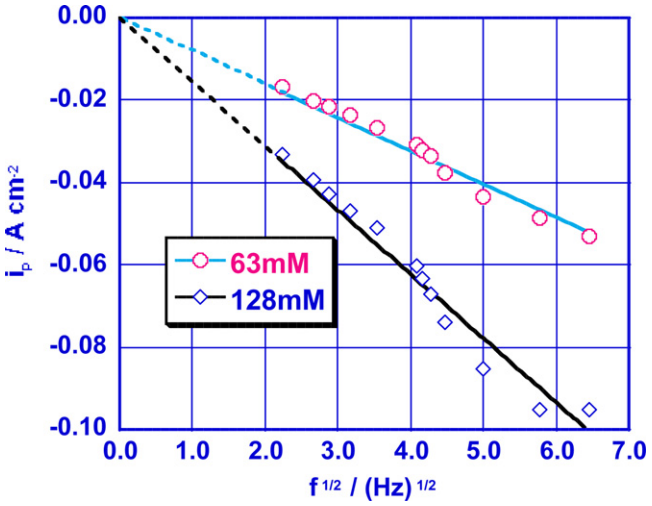

Fig. 11. The linear relationship between square wave peak current (a) and square root of frequency. Ce(III) ion concentration was 128 mM.

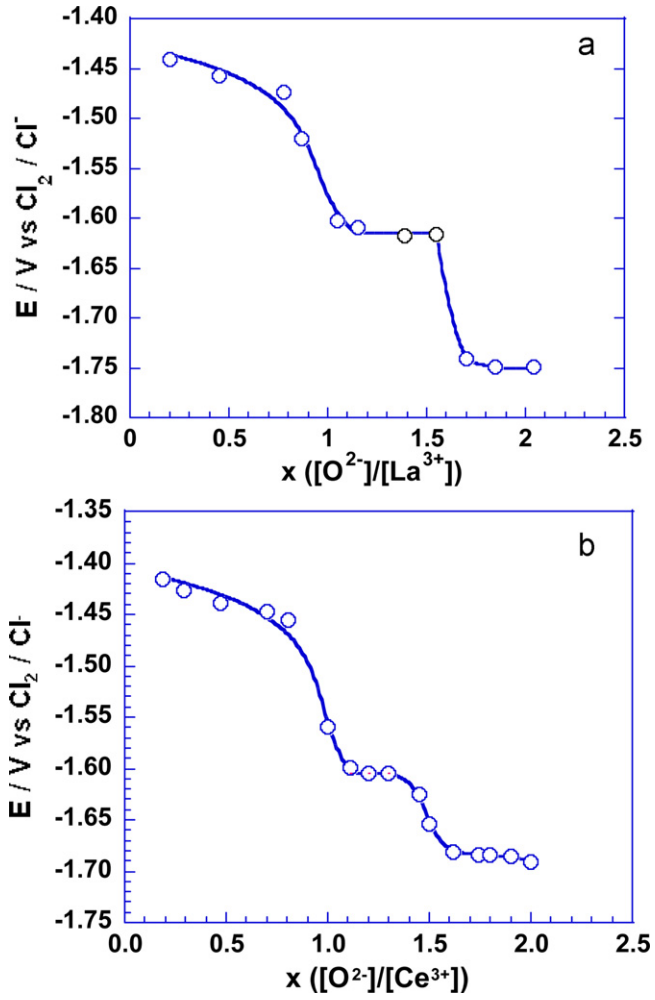

Fig. 12. The potentiometric-titration plot of La(III) ions with an initial concentration of 310 mM (a) and Ce(III) ions (b) with an initial concentration of 280 mM in a NaCl–2CsCl melt at a temperature 873 K.

Eq. (2) can be applied in the frequency range studied. Furthermore, the diffusion coefficient of Ce(III) ions in NaCl–2CsCl at 873 K can be calculated as 7.17×10^{-5} cm^2 s^{-1}, which has the same order of magnitude as determined by cyclic voltammetry.

Table 1
The solubility of MOCl and M_2O_3.

	LaOCl	La_2O_3	CeOCl	Ce_2O_3
pK_s	5.31	11.07	5.17	11.02

The best chlorinating condition could be extracted from the comparison of the E-pO^{2-} diagram corresponding to the M–O compounds and that of some chlorinating mixtures. The identification of the M–O (M = La, Ce) compounds that are stable in the NaCl–2CsCl melt, as well as the determination of their solubility products, was carried out by potentiometric titration using an oxide ion sensor. Rare earth ions M(III) (M = La, Ce) are precipitated as an oxide, and when the reaction is monitored with the zirconia electrode selective to O^{2-} ions, an *emf* jump occurs at the point corresponding to the stoichiometric precipitation of the oxide. The potential values are obtained after successive additions of known amounts of NaOH to the solutions of La(III) and Ce(III) with initial concentrations of 280 mM and 310 mM, respectively. The corresponding results are shown in Fig. 12. From the titration curves of Ce(III) and La(III), two *emf* jumps occur respectively at the point *x* (defined as the ratio of added oxide ions to the initial M(III) concentration) equal to 1 and 1.5. It is clear that MClO and M_2O_3 are two solid stable compounds in the melts studied. The reactions are as follows:

$$M(|||) + O^{2-} + Cl^- = MOCl(s) \quad (6)$$

$$M(|||) + 3O^{2-} = M_2O_3(s) \quad (7)$$

The data was analysed by using the following theoretical equation, and by assuming that no M_2O_3 is formed:

$$E = E^0 + \frac{2.3RT}{2F}\left[-\log\frac{c_0(x-1)+\sqrt{c_0^2(x-1)^2+4k_{s(MOCl)}}}{2}\right] \quad (8)$$

where C_0 is the initial concentration of M(III), E^0 and the solubility product of MOCl, and $k_{s(MOCl)}$ can be obtained by fitting the theoretical equation with the experimental data. Furthermore, the solubility product of M_2O_3 ($K_{s(M_2O_3)}$) can be calculated by relationship (9), defined by the mass balance Eq. (10).

$$\frac{k^2_{s(M_2O_3)}}{k_{s(MOCl)}} = \frac{1}{[O^{2-}]} \quad (9)$$

$$2MOCl + O^{2-} = M_2O_3 + 2Cl^- \quad (10)$$

Table 2
The standard potential values of a redox system with rare earths in a NaCl–2CsCl mixture at 873 K.

System	Expression for equilibrium potential calculation	Corresponding E^0 of M/V *vs* Cl_2/Cl^-	
		La	Ce
M^{3+}/M^{2+}	E_1^0	–	−2.52
M^{2+}/M	E_2^0	–	−2.97
M^{3+}/M	E_3^0	−3.01	–
$MOCl/M^{2+}$	$E_4^0 = E_1^0 - \frac{2.3RT}{F}pK_{s(MOCl)}$	–	−3.41
$M_2O_3/2M^{2+}$	$E_5^0 = E_1^0 - \frac{2.3RT}{2F}pK_{s(M_2O_3)}$	–	−3.49
MOCl/M	$E_6^0 = E_3^0 - \frac{2.3RT}{3F}pk_{s(MOCl)}$	−3.29	–
$M_2O_3/2M$	$M_2O_3(s) + Cl_2(g) + Na_2O(s) = 2MO_2(s) + 2NaCl(s)$		
	$E_7^0 = \frac{\Delta G_7^*}{6F} - \frac{2.3RT}{F}\log a_{NaCl} + \frac{2.3RT}{2F}\log \gamma_{Na_2O}$	−3.42	−3.22
$2MO_2/M_2O_3$	$La_2O_3(s) + Cl_2(g) + Na_2O(s) = 2LaO_2(s) + 2NaCl(s)$		
	$E_8^0 = \frac{\Delta G_8^*}{2F} - \frac{2.3RT}{F}\log a_{NaCl} + \frac{2.3RT}{F}\log a_{Na_2O}$	−1.71	−1.73
$MO_2/MOCl$	$E_9^0 = E_8^0 + \frac{2.3RT}{2F}\frac{pk^2_{s(MOCl)}}{pk_{s(M_2O_3)}}$	−1.63	−1.65
MO_2/M^{3+}	$E_{10}^0 = E_9^0 - \frac{2.3RT}{F}pk_{s(MOCl)}$	−2.54	−2.54

*The Gibbs energy (ΔG) was calculated through thermodynamic data from Refs. [22,23], a_{NaCl} and γ_{Na_2O} have been derived from the literature data [22].

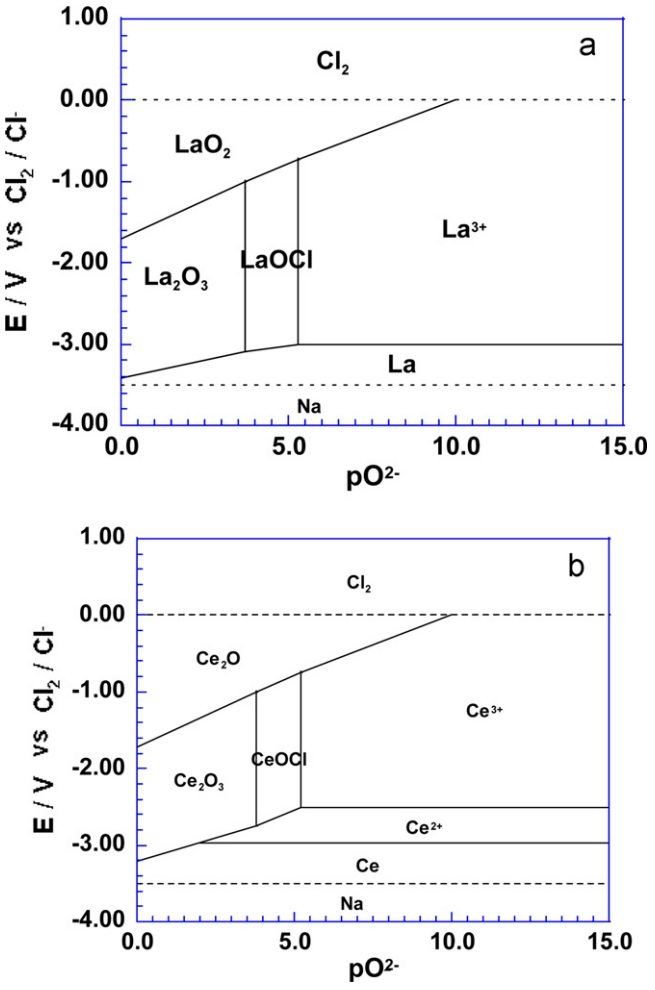

Fig. 13. The E-pO^{2-} diagrams of Lanthanum (a) and Cerium (b) in a NaCl–2CsCl melt.

The corresponding fitted and calculated results are shown in Table 1.

In order to construct a diagram for M–O compounds in a NaCl–2CsCl mixture, a series of physical chemical data must be obtained, and Table 2 gives the necessary data [22,23]. The standard potentials were deduced from linear extrapolation of the plots between *emf* and logarithm of M(III) concentration, at a MCl_3 concentration equal to 1 mol kg^{-1}. With the solubility products of the M–O compounds and the equilibrium potentials of the different redox couples involved, it is possible to establish the E-pO^{2-} diagram (Fig. 13).

4. Conclusion

The electrochemical behavior of rare earth ions in NaCl–2CsCl (mole ratio) was investigated using cyclic voltammetry and square wave voltammetry on a tungsten electrode. The two electrochemical methods yield similar results, in that: for La(III) ions, the cathodic process is a direct $La^{3+} + 3e^- = La$ step, which is similar to the results studied in other chloride melts; and for Ce(III) ions, the cathodic process of cerium ions in the studied melt consists of two reversible steps: $Ce^{3+} + e^- = Ce^{2+}$ and $Ce^{2+} + 2e^- = Ce$. Furthermore, the electrokinetics of Ce(III) ions was investigated in detail in NaCl–2CsCl melts, and it was noticeable that the values of the diffusion coefficient obtained by the two methods are in the same order of magnitude. Moreover, a magnesia stabilised zirconia tube with an inner reference of Cr/Cr_2O_3 was used as the oxide sensor, to potentiometrically titrate the solubility products of the M–O compounds (M = La, Ce) in the NaCl–2CsCl molten salt. Two stable M–O compounds, MOCl and M_2O_3, were observed in the titration plot. The solubility products ($k_{s(MOCl)}$ and $K_{s(M_2O_3)}$) were obtained through fitting and calculating of obtained experimental data. Also, a E-pO^{2-} diagram for M–O stable compounds had been constructed by combining both theoretical and experimental data.

Acknowledgments

The work was supported by the National Nature Science Foundation of China (no 51004008, no 21071014) and the Program for Changjiang Scholars and Innovative Research Team in University (no. IRT0708). The authors appreciate Dr K.T. Kilby at University of Cambridge for his useful discussion and great helps.

References

[1] R.J.M. Konings, J.L. Kloosterman, A view of strategies for transmutation of actinides, Prog. Nucl. Energy 38 (2001) 331–334.
[2] C. Madic, M.J. Hudson, J.O. Liljjenzin, J.P. Glatz, R. Nannicini, A. Facchini, Z. Kolarik, R. Odoj, Recent achievements in the development of partitioning processes of minor actinides from nuclear wastes obtained in the frame of the NEWPART European programme (1996–1999), Prog. Nucl. Energy 40 (2002) 523–526.
[3] T. Ogawa, M. Akabori, F. Kobayashi, R.G. Haire, Thermochemical modeling of actinide alloys related to advanced fuel cycles, J. Nucl. Mater. 247 (1997) 215–221.
[4] V.A. Volkovich, T.R. Griffiths, R.C. Thied, Treatment of molten salt wastes by phosphate precipitation: removal of fission product elements after pyrochemical reprocessing of spent nuclear fuels in chloride melts, J. Nucl. Mater. 323 (2003) 49–56.
[5] Y. Gohar, FLIBE blanket concept for transmuting transuranic elements and long-lived enriched uranium, Fusion Eng. Des. 58–59 (2001) 1097–1101.
[6] I. Johnson, C.E. Johnson, Light element thermodynamics related to actinide separations, J. Nucl. Mater. 247 (1997) 177–182.
[7] J.P. Grouiller, S. Pillon, C.S. Jean, F. Varaine, L. Leyval, G. Vambenepe, B. Carlier, Minor actinides transmutation scenario studies with PWRs, FRs and moderated targets, J. Nucl. Mater. 320 (2003) 163–169.
[8] M. Iizuka, T. Inoue, O. Shirai, T. Iwai, Y. Arai, Application of normal pulse voltammetry to on-line monitoring of actinide concentrations in molten salt electrolyte, J. Nucl. Mater. 297 (2001) 43–51.
[9] Y. Castrillejo, M.R. Bermejo, R. Pardo, A.M. Martínez, Use of electrochemical techniques for the study of solubilization processes of cerium-oxide compounds and recovery of the metal from molten chlorides, J. Electroanal. Chem. 522 (2002) 124–140.
[10] C. Caravaca, P. Díaz Arocas, J.A. Serrono, C. González, Solubilization studies of rare earth oxides and oxyhalides: application of electrochemical techniques in pyrochemcial process, in: 6th Exchange Meeting Proceeding, Mould, Spain, 2000, pp. 625–636.
[11] M. Iizuka, T. Koyama, N. Kondo, R. Fujita, H. Tanaka, Actinides recovery from molten salt/liquid metal system by electrochemical methods, J. Nucl. Mater. 247 (1997) 183–190.
[12] L.R. Morss, M.A. Lewis, M.K. Richmann, D. Lexa, Cerium, uranium, and plutonium behavior in glass-bonded sodalite, a ceramic nuclear waste form, J. Alloys Compd. 303–304 (2000) 42–48.
[13] K. Serrano, P. Taxil, O. Dugne, S. Bouvet, E. Puech, Preparation of uranium by electrolysis in chloride melt, J. Nucl. Mater. 282 (2000) 137–145.
[14] Y. Sakamura, T. Hijikata, K. Kinoshita, T. Inoue, T.S. Storvick, C.L. Krueger, J.J. Roy, D.L. Grimmett, S.P. Fusselman, R.L. Gay, Measurement of standard potentials of actinides (U, Np, Pu, Am) in LiCl–KCl eutectic salt and separation of actinides from rare earths by electrorefining, J. Alloys Compd. 271–273 (1998) 592–596.
[15] J. Serp, R.J.M. Konings, R. Malmbeck, J. Rebizant, C. Scheppler, J.P. Glatz, Electrochemical behaviour of plutonium ion in LiCl–KCl eutectic melts, J. Electroanal. Chem 561 (2004) 143–148.
[16] P. Chamelot, B. Lafage, P. Taxil, Using square-wave voltammetry to monitor molten alkaline fluoride baths for electrodepositions of niobium, Electrochim. Acta 43 (1997) 607–616.
[17] J. De Strycker, P. Westbroek, E. Temmerman, Electrochemical behaviour and detection of Co(II) in molten glass by cyclic and square wave voltammetry, Electrochem. Commun. 4 (2002) 41–46.
[18] J. O'Dea, J. Osteryoung, R.A. Osteryoung, Theory of square wave voltammetry for kinetic systems, Anal. Chem. 53 (1981) 695–701.
[19] J.H. Christle, J.A. Turner, R.A. Osteryoung, Square wave voltammetry at the dropping mercury electrode: theory, Anal. Chem. 49 (1977) 1899–1903.
[20] L. Ramaley, M.S.J. Krause, Theory of square wave voltammetry, Anal. Chem. 41 (1969) 1362–1369.
[21] G.C. Barker, Square wave polarography and some related techniques, Anal. Chim. Acta 18 (1958) 118–130.
[22] J. Lumsden, Thermodynamics of Molten Salt Mixture, Academic press Inc., London, 1966.
[23] D.L. Ye, The Handbook of Thermodynamics Data, Yejin Gongye Press, Beijing, 1981.